Bulletin of the New Zealand Society for Earthquake Engineering, Vol. 49, No. 4, December 2016

AXIAL ELONGATION IN DUCTILE REINFORCED CONCRETE WALLS

Ericson Encina[1], Yiqiu Lu[1] and Richard S. Henry[2]

(Submitted *July 2016*; Reviewed *August 2016*; Accepted *October 2016*)

ABSTRACT

Axial elongation has been observed during tests of reinforced concrete (RC) members subjected to either monotonic or cyclic loading. The implications of elongating plastic hinges in beams on the seismic performance of RC frame buildings, and in particular the floor systems, has been extensively studied. However, few investigations have addressed axial elongation of RC walls. To expand on the existing knowledge of axial elongation in RC members, the measured axial elongations of 13 previously tested RC walls were investigated. These tests included a wide range of vertical reinforcement ratios, vertical reinforcement layouts, and axial loads. The procedures to estimate wall elongation that were proposed in the Public Comment Draft Amendment No. 3 of the New Zealand Concrete Structures Standard (NZS 3101:2006) were also evaluated and compared against the measured elongations from the tests. The experimental results showed that elongation magnitudes in the analysed walls were between 0.4-0.8% of the wall length at 1.5% lateral drift, and that the elongation equations proposed for NZS 3101:2006 provided an acceptable estimation of the expected elongation in RC walls. Additionally, numerical models were developed using distributed-plasticity fibre-based elements in OpenSees and membrane elements in VecTor2 to verify the ability of these commonly used modelling techniques to capture wall elongation. The numerical simulations were able to represent the global and local behaviour with good accuracy and both models were able to capture the peak elongations. However, the more sophisticated concrete material models in OpenSees allowed the fibre element models to more accurately represent the experimental wall elongations, especially when considering residual elongations.

INTRODUCTION

Current seismic design philosophies rely on ductility to allow buildings to resist the demands imposed by large earthquakes with a low probability of collapse. In the case of reinforced concrete (RC) structures, ductility is achieved by detailing the expected plastic hinge regions and implementing capacity design principles. The plastic hinge regions of RC members have been proven to increase in length when subjected to cyclic displacements, which is commonly referred to as axial elongation [1].

Axial elongation in RC members has been extensively studied in New Zealand since the early 1980s. Research conducted at the Universities of Auckland and Canterbury has resulted in a fundamental understanding of how to estimate plastic hinge elongation and its effect on adjacent building components. Experimental research has given particular attention to the interaction between beams and columns [2-5] and the interaction between floors and elongating beams [6-9]. In addition, numerical research has focused on prediction of elongation based on plastic hinge models [7, 10, 11] and the effects of beam elongation on structural systems [10, 12]. This prior research has led to a sound understanding of the mechanics of plastic hinge elongation.

In ductile RC walls, plastic hinges are typically designed to form at the wall base. Under a severe seismic excitation, the inelastic rotations in these hinges will result in axial elongations that cause the wall to increase in height. The elongation generated in the wall plastic hinge could be restrained by surrounding structural elements, such as floors, beams and columns. Interaction between these structural systems may alter the loads induced in the wall as well as the other elements that the walls are coupled to. This phenomenon was previously observed and reported during a joint U.S. and Japan project in the early 1980s that involved testing a 7-storey RC building composed by a wall and perimeter frames [13]. Researchers found that the lateral strength of the test building was significantly higher than the design capacity that was estimated prior to testing. The outrigger effect generated by the coupling between the gravity frame and the wall, plus the elongation of the wall plastic hinge, were found to significantly contribute to the amplification of shear and axial demands acting on the wall as well as the increase in the lateral load system capacity. A numerical study by Chesi and Schnobrick [14] captured the vertical load redistribution between the gravity system and the wall and accurately simulated the experimental wall response. These studies highlighted the importance of considering structural interaction and wall plastic hinge elongation when analysing the lateral load response of building systems.

Axial elongation of RC wall plastic hinges has received little attention in both practice and research. The effect of elongation on axial loads in RC walls was highlighted by both the Canterbury Earthquakes Royal Commission [15] and in the SESOC Interim Guidelines [16]. Prior to the Canterbury Earthquakes, explicit provisions to account for plastic hinge elongation in RC walls was not considered by concrete design standards, but recent amendments have been proposed to the New Zealand Concrete Standard which include simplified equations to estimate axial elongation in different members [17]. Verification of these proposed provisions and experimental research to determine the likely magnitude of elongation in walls and its interaction with surrounding

[1] *Doctoral Candidate, University of Auckland, Auckland, correspondence to Ericson Encina eenc456@aucklanduni.ac.nz.*
[2] *Senior Lecturer, University of Auckland, Auckland*

elements has not yet been fully considered. Consequently, there is a general lack of understanding as to the extent of axial elongation of RC walls and how this could be included when analysing and designing buildings.

An investigation was conducted to analyse the axial elongations that were measured from 13 previously tested RC walls. Axial elongations in these test walls were analysed and modelled to assess the typical magnitude of these elongations and to verify the ability of commonly used numerical modelling techniques to simulate elongation in RC walls.

BACKGROUND ON PLASTIC HINGE ELONGATION

In the late 1970s plastic hinge elongation was observed during research that focused on the behaviour of RC beams subjected to cyclic loading [18]. Based on cantilever beam tests, Fenwick and Thom [19] provided an explanation for the axial elongation of RC plastic hinges. Fenwick and Megget [1, 20] studied the elongation produced on unidirectional and reversing plastic hinges under a variety of scenarios. These investigations provided the basis of the current understanding of the mechanics of elongation in RC plastic hinges.

Elongation in RC plastic hinges occurs due to the mechanics of flexural resistance in RC sections [1, 18-20]. Typically, the elongation is measured at the mid-section of a member as illustrated in Figure 1, and so any strain profile where the neutral axis depth differs from the centreline of the section will produce a net elongation, referred to as geometric elongation. Under a specific lateral displacement history, the elongation trends are dictated by the type of plastic hinge – reversing or uni-directional – and the magnitude of the strains in the reinforcement. As an example, Figure 2 illustrates the elongation development of two beams by plotting the axial deformations in the top and bottom flexural reinforcement over the length of the plastic hinge at different load stages [1]. It can be seen that in a unidirectional plastic hinge (Figure 2a) compression strains are negligible compared to tensile strains [20, 21], therefore the rotation of the plastic hinge, and so the elongation, depends mainly on the magnitude of the reinforcement tensile strains. However, in reversing plastic hinges (Figure 2b), the top and bottom reinforcement both extend during cyclic loading. In this case the elongation depends on the average extension of the reinforcement at both ends of the section plus the geometric elongation [1].

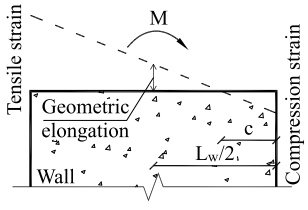

Figure 1: Geometric elongation in an RC member.

In addition to the geometric elongation and as a consequence of the cracking of the concrete matrix some cracks may remain open upon load reversal. These residual crack widths are caused by two mechanisms [19], namely the contact stress effect and truss action effect, both illustrated in Figure 3. The former is produced by dislodged concrete particles that fall into the cracks. This debris could be produced by either the cracking process or pulled into the open cracks by the ribs of the straining bars [19]. Upon load reversal the dislodged particles tend to limit the crack closure and act as wedges, especially when shear displacements contribute to imperfect matching between opposite crack surfaces [19]. The latter arises from the shear transfer mode in plastic hinges, where most of the shear is transferred by diagonal concrete struts. To satisfy equilibrium at any cross section within the plastic hinge the flexural tension force must be equal to the flexural compression force plus the vertical component of the inclined compression strut, as shown in the forces at section A-A in Figure 3 [19]. This mechanism results in lower compression stresses in the reinforcement than those produced in tension during the previous cycle and so plastic tensile strains cannot be fully recovered when the load is reversed

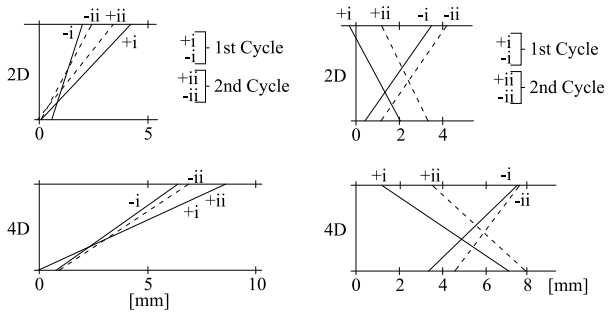

(a) Uni-directional plastic hinge. *(b) Reversing plastic hinge.*

Figure 2: Axial deformation profiles in RC beam plastic hinges (After Fenwick and Megget [1]).

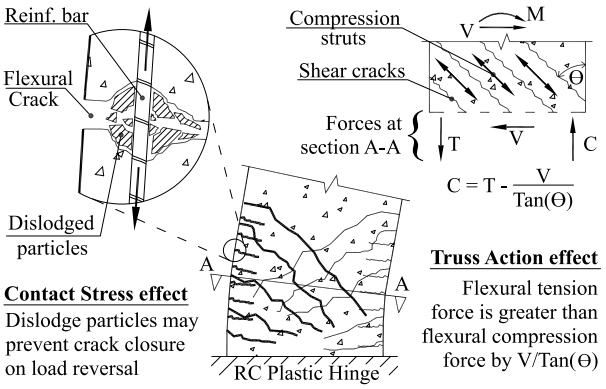

Figure 3: Causes of residual crack widths in the plastic hinge.

The plot in Figure 4 presents the development of elongation in an RC beam plastic hinge [11]. As shown in the figure, the elongation process is continuous and cumulative during cyclic displacements. The isolated half cycle on the right shows the process in detail: starting from the previous residual elongation, then elongating due to geometric elongation and finally, on the way back, only a portion of the geometric elongation is recovered, adding to the pre-existing residual crack widths. Research has also shown that the irrecoverable portion of the elongation may be reduced when axial load is applied to the specimens [22]. It is worth noting that any physical restraint to elongate could be translated into axial load acting on the plastic hinge that may reduce the net elongation.

Previous numerical studies have focused on predicting beam elongation and the effect of elongating plastic hinges on the seismic behaviour of framed structures. Numerical models developed to predict axial elongation of RC plastic hinges have included simplified empirical equations [23, 24] and numerical models aimed for finite element software [7, 10, 11, 25-28]. In general, the technique used in most of the models was to represent the plastic hinge length with a multi-spring or fibre-based approach, and in some models, include shear

response within the plastic hinge through diagonal elements [11, 28].

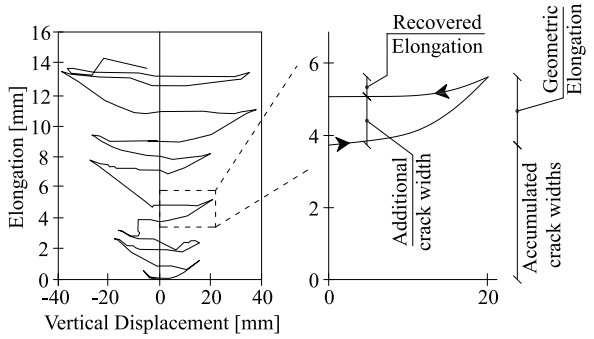

Figure 4: Elongation development in an RC beam (Adapted from Peng et al. [11]).

Elongation provisions have recently been included in the proposed Public Comment Draft Amendment No. 3 of the New Zealand Concrete Structures Standard (NZS 3101:2006) [17]. The provisions highlight the importance of axial elongation of plastic hinges and also provide guidance on estimating elongations in different RC members. For RC walls, the magnitude of the elongation (E_l) measured at the mid-section at the ultimate limit state (ULS) shall be determined using the Equation 1, where θ_p is the plastic rotation of the hinge, L_W is the length of the wall, and c is the neutral axis depth at ULS. The elongation at any other fibre of the section can be determined by adding the extra deformation due to rotation to the elongation at mid-section. It is worth noting that the estimation of wall elongation through Equation 1 accounts just for the geometrical elongation produced by the plastic rotation of the plastic hinge, with the axial load expected to minimise any permanent elongation.

$$E_l = \theta_p \left(0.5L_W - c \right) \quad (1)$$

Additionally, the proposed amendment states that for an MCE event the magnitude of the elongation shall be considered as 1.5 times the corresponding elongation at ULS, with a maximum of 3.6% of the length of the wall.

REINFORCED CONCRETE WALL TESTS

In order to investigate plastic hinge elongation in ductile rectangular RC walls, three series of previously tested walls were selected that are referred to as PW, RW and C series. The selection was based on walls that were representative of current New Zealand construction practice in tall buildings as well as the availability of reliable experimental data. The 13 individual walls in all three test series were subjected to reverse cyclic loading until failure.

PW Series: PW1 to PW4

The PW walls were representative of the lower 3 levels of a one-third scaled 10-storey RC wall. The test walls were 152 mm thick, 3048 mm long and 3657 mm tall, and were subjected to cyclic lateral displacement. In addition to the self-weight, a nominal load equal to an axial load ratio, ξ, of 10.0% was applied at the top of the specimens. A detailed description of the tests can be found in Birely [29] and Lowes et al. [30].

Details of the PW wall reinforcement detailing is shown in Figure 5. Walls PW1, PW2 and PW4 had lumped vertical reinforcement (reinforcement ratio of 3.4%) at both ends of the wall and minimum vertical reinforcement (reinforcement ratio of 0.27%) in the web region. The end region of these walls had vertical reinforcement that consisted of 7 rows of 3×12.7 mm diameter bars confined by 6.35 mm diameter stirrups and cross ties spaced at 51 mm centres. Vertical and horizontal reinforcement in the web consisted in 2 layers of 6.35 mm diameter bars spaced at 152 mm. Wall PW3 had uniformly distributed vertical reinforcement over the wall section. Vertical reinforcement consisted of 2 layers of 12.7 mm diameter reinforcement spaced at 108 mm (steel ratio 1.54%) centres and transverse reinforcement was 6.35 mm diameter reinforcement spaced at 152 mm centres. Two additional vertical bars (12.7 mm diameter) were included in each wall end (reinforcement ratio of 2.01%). Confinement of the wall ends was provided by 6.35 mm diameter stirrups and cross ties at 44 mm on centres. Splices were not used in the specimens, except in PW4 where the vertical reinforcement was spliced right above the wall-foundation interface.

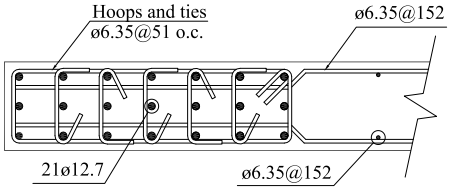

(a) PW1, PW2 and PW4.

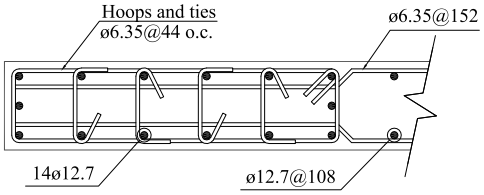

(b) PW3.

Figure 5: Wall reinforcement detailing for PW walls (mm).
Note: The 90-degree anchorage of cross ties is not compliant with NZS 3101:2006.

Combinations of axial, moment and shear forces were applied at the top of the specimens to represent the equivalent demand that is produced at that level when the 10-storey wall is subjected to a specific load pattern. The load pattern for PW1 was the equivalent lateral force pattern described in ASCE7-05 [17], and the load pattern for the rest of the walls was the uniformly distributed lateral load. The loading protocol consisted in symmetrical reversed cyclic lateral displacement up to 1.5% drift.

The nominal concrete strength for all the PW walls was 34.5 MPa and the nominal reinforcement yield strength was 420 MPa. Actual material properties measured for each specimen can be found in the literature [29].

RW Series: RWN, RWC and RWS

The walls in this series represented a half-scaled 4-storey RC wall. They had an asymmetric vertical reinforcement layout intended to simulate the flexural behaviour of T-shaped walls [31, 32]. The three walls were identical except that different methods of splicing the vertical reinforcement were considered. RWN had no splice in the vertical reinforcement, RWC used couplers right at the wall-foundation interface, and RWS used a typical lap splice above the wall-foundation interface.

The RW specimens were 152 mm thick, 2286 mm long and 6400 mm tall and the reinforcement detailing is shown in Figure 6. The walls had lumped reinforcement in the end of the wall and distributed reinforcement in the web region.

Vertical reinforcement in the left wall end consisted of 4×19 mm and 2×16 mm diameter reinforcement with 6.35 mm diameter stirrups and cross ties spaced at 64 mm centres. Vertical reinforcement in the right wall end consisted of 8×28.7 mm diameter bars, the outmost 4 bars were confined by 6.35 mm diameter stirrups spaced at 51 mm centres. Vertical reinforcement in the web region consisted of two layers of 12.7 mm diameter bars spaced at 458 mm centres. The horizontal reinforcement of the wall consisted in 2 layers of 9.5 mm diameter bars spaced at 190 mm centres.

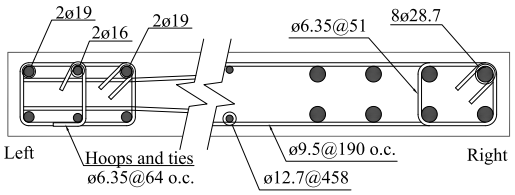

Figure 6: Wall reinforcement detailing for RW walls (mm).

The loading protocol for the RW walls consisted of a single lateral load applied at a height of 6096 mm above wall-foundation interface. The load subjected the wall to symmetric reversed cycles up until 1.0% lateral drift and asymmetric displacements were applied thereafter up to 2.5% when the left wall end was in tension. Besides the self-weight of the wall, there was no additional axial load applied to any of the walls during testing.

The RW walls were cast in 2 lifts up the wall height. The nominal concrete strength was 34.5 MPa and the nominal reinforcement yield strength was 420 MPa. The full measured material properties for each wall can be found in the literature [31].

C Series: C1 to C6

The test walls represented the lower levels of a 40-50% scaled multi-storey flexural-dominant RC wall with limited ductility in accordance with NZS3101:2006 [33]. The key parameters in this investigation were axial load ratio (ξ), shear-to-span ratio ($M_b/(V_b \times l_w)$) and the transverse reinforcement in the wall end.

The C walls were 150 mm thick, 1400 mm long and 2800 mm tall and the reinforcement detailing is shown in Figure 7. The walls had uniformly distributed vertical reinforcement consisting on 2 layers of 7×10 mm diameter bars spaced at 225 mm centres. The horizontal reinforcement consisted in 6 mm diameter bars spaced at 150 mm centres throughout the wall height. Additionally, walls C5 and C6 were provided with confinement stirrups at the ends of the walls that consisted of 6 mm diameter stirrups spaced at 90 mm and 60 mm centres, respectively. The end of the wall confinement extended up to 1400 mm above the wall-foundation interface. The vertical reinforcement was continuous from the bottom to the top of the walls.

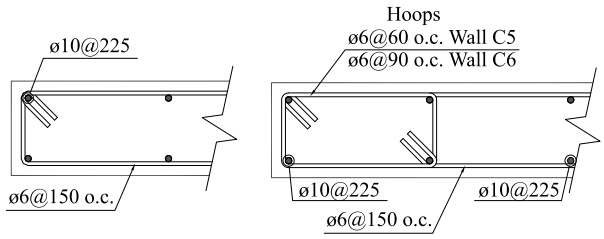

(a) Wall C1 to C4. *(b) Wall C5 and C6.*

Figure 7: Wall reinforcement detailing for C walls (in mm).

Combinations of axial, moment and shear forces were applied at the top of the test walls to simulate the actions produced in a multi-storey building. The shear-to-span ratios analysed were 2, 4, or 6. The loading protocol subjected the walls to reversed cyclic lateral displacements up until failure at 2.5% drift. In addition to the self-weight, constant nominal axial load was applied to the walls that ranged between no additional axial load and up to an axial load ratio ξ = 7%. The axial load and shear span ratios were kept constant throughout each test.

Nominal concrete compressive strength was 40 MPa. Nominal steel yield stress was 300 MPa. Actual material properties for each specimen can be found in the literature [33].

EXPERIMENTAL RC WALL ELONGATION

Elongation History

Figure 8, Figure 9, and Figure 10 illustrate the history of measured cyclic axial elongations during six of the tests from the PW, RW, and C series, respectively. The six selected walls shown are PW1, PW2, RWN, C1, C4 and C5 and represented key variations to compare the elongation behaviour between the tests.

The development of elongation in the PW walls (Figure 8) progressed symmetrically and increased as the wall lateral displacement increased. Irrespective of the lateral load pattern (inverted triangular for PW1 and uniform for PW2) the elongation cycled back and forth following similar paths throughout the tests. There was a noticeable lack of accumulation of residual cracks widths during repeated cycles for all of the PW specimens, with the elongation history tracing an almost linear path. An exception occurred close to the end of the tests when, for example, PW1 developed some residual elongation while PW2 did not, highlighting the influence of the axial load and the particular damage sustained by each specimen at failure.

The typical history of axial elongation for the RW walls, represented by wall RWN is shown in Figure 9. The elongation increased as lateral displacement increased, but developed asymmetrically for loading in each direction. Axial elongations were greater when the walls were displaced to positive lateral drifts, because when the end of the wall with less vertical reinforcement was in tension, the neutral axis was less, producing higher tensile strains and elongations. Then when loaded on the opposite direction, the more heavily reinforced end of the wall in tension demanded a deeper neutral axis, reducing the tensile strains and elongation. Unlike the PW walls, the absence of axial load allowed for unrestrained elongation of the RW walls, with an elongation history that more closely resembled that of a beam. Residual elongations had a moderate contribution to the total elongation of the specimens. Additionally, the repetitive cycles (9 times) at -1.0% lateral drift caused a slight increase in both peak displacement elongation and residual elongation.

The elongation histories of three of the C walls that had the same shear span and varying axial loads are shown in Figure 10. Similar to the PW walls, the cyclic development of the elongation progressed symmetrically and increased with lateral displacement. In these tests the axial load had a significant influence in the development of axial elongations. Wall C4 with no axial load showed a large accumulation of elongations, with only minor recovery during reverse cycles. The moderate axial load applied to wall C1 reduced the residual elongations and the higher axial loads applied to C5 resulted in an almost linear elongation history. In general, the lightly reinforced concrete walls developed larger elongations than the more heavily reinforced concrete walls. Additionally, the lack of flexural crack distribution resulted in concentrated

reinforcement strains that would have increased the residual elongations that developed. It is worth noting that the elongation developed by C1 as a percentage of the wall length was larger than that for RWN even when C1 had an axial load ratio of 3.5% and RWN had just its self-weight.

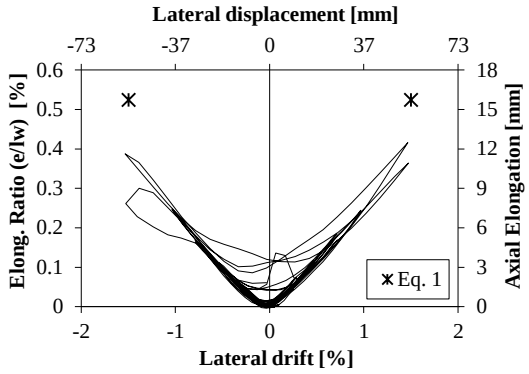

(a) Wall PW1 (ξ=9.6%).

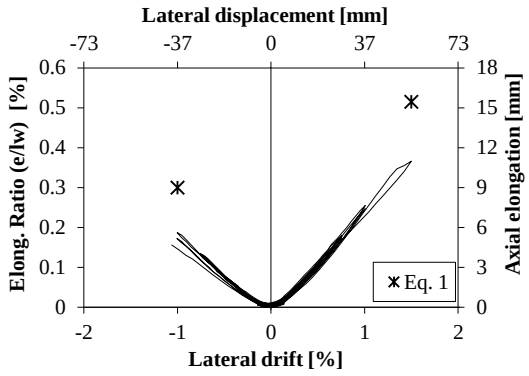

(b) Wall PW2 (ξ=13%).

Figure 8: Elongation development for PW walls.

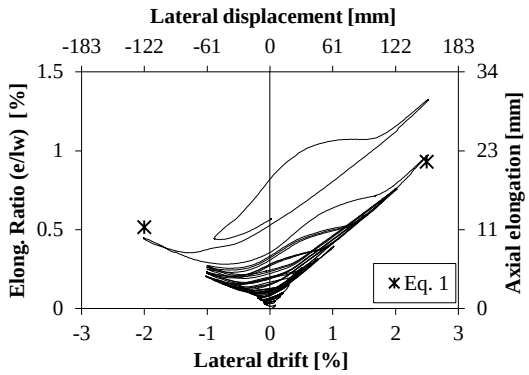

Figure 9: Elongation development for RWN (ξ=0%).

NZS 3101:2006 Elongation Estimate

The estimate of elongation using Equation 1 from the proposed amendment 3 to NZS 3101:2006 at the maximum test drifts is presented as an asterisk for each wall in Figure 8, Figure 9, and Figure 10. The elongation estimates were calculated using plastic hinge lengths (l_p) and yield curvatures (θ_y) from NZS3101:2006, plastic rotations based on $\theta_p = \theta_{Total} - \theta_y$, and neutral axis depth (c) obtained from a sectional analysis [34]. These key parameters used for the elongation calculations are summarised in Table 1.

The elongation estimates using Equation 1 matched the data with reasonable accuracy. For the analysed walls the predicted elongations were within a range of ±5mm from the experimentally measured elongation. In general, elongations were over-estimated for walls with higher axial loads (PW walls) and underestimated the elongations for the lightly reinforced walls with low or no axial loads (C1, C4). This was not surprising given that the simplified estimation accounts for only the geometric component of elongation.

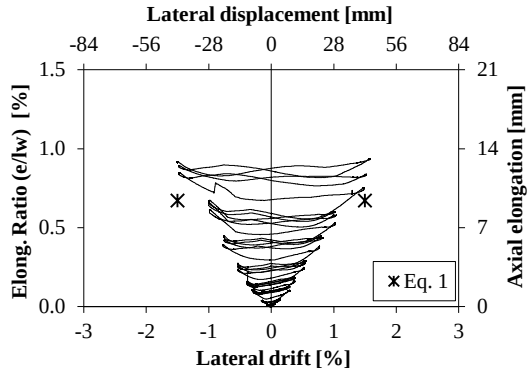

(a) Wall C4 (ξ=0.0%).

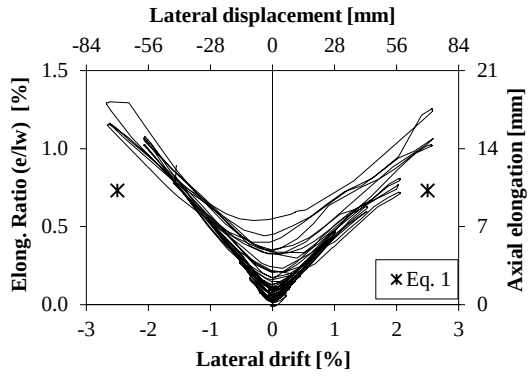

(b) Wall C1 (ξ=3.5%).

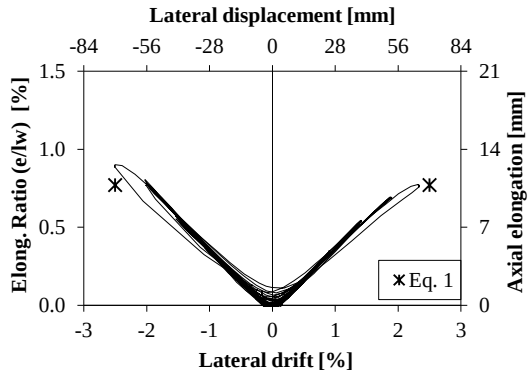

(c) Wall C5 (ξ=7.5%).

Figure 10: Elongation development for C walls.

Table 1: Elongation prediction by Equation 1.

Wall	Drift [%]	θ_p [rad]	c [mm]	E_l [mm]	E_l/L_W [%]
PW1	±1.5	0.0165	537	16.3	0.53
PW2	+1.5	0.0159	555	15.5	0.51
PW2	-1.0	0.0101	622	9.2	0.30
RWN +	+2.5	0.0253	326	20.7	0.91
RWN -	-2.0	0.0199	555	11.7	0.51
C1	±2.5	0.0262	310	10.2	0.73
C4	±1.5	0.0261	88	9.4	0.67
C5	±2.5	0.0261	289	10.8	0.77

Peak and Residual Cyclic Elongations

The axial elongations at the peak of each load cycle are plotted for all 13 test walls in Figure 11 to Figure 13. The peak elongations that developed in the PW walls (Figure 11) were relatively consistent between the test specimens. With the exception of the small force controlled drift cycles up to ±0.3%, the elongation increased linearly with drift. Variations on load pattern, vertical reinforcement layout, and splice method did not appear to have any significant impact on the elongation magnitudes or trends. The high axial loads applied to the PW walls resulted in relatively low peak elongations that ranged between 0.22% and 0.25% of the wall length at ±1.0% lateral drift.

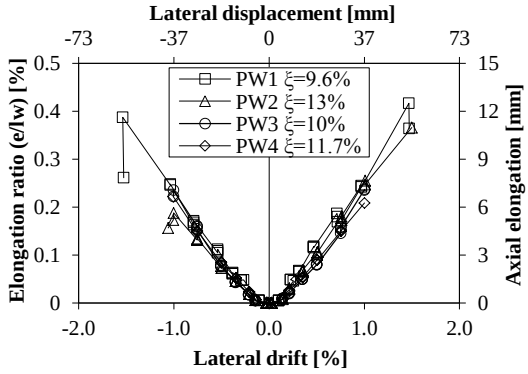

Figure 11: Peak elongations for PW walls.

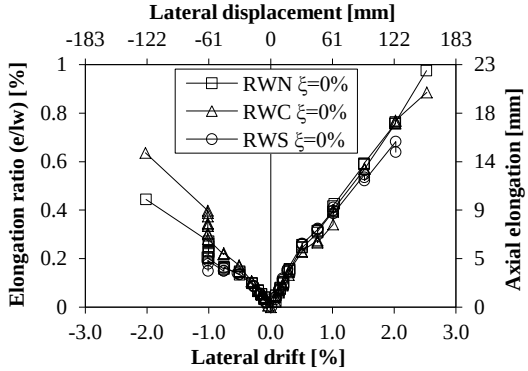

Figure 12: Peak elongations for RW walls.

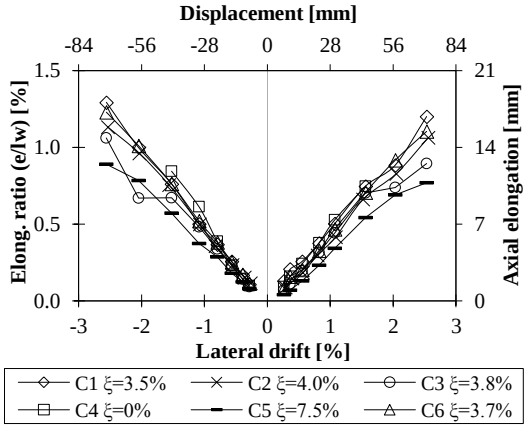

Figure 13: Peak elongations for C walls.

The peak elongations for the RW walls (Figure 12) progressed asymmetrically and increased during repetitive cycles to -1.0% drift for the three walls. In general, the peak elongation was relatively consistent for all three walls, but in the case of negative drifts RWC developed higher peak elongations than RWN and RWS. Additionally, for positive displacements elongation followed a fairly linear trend with drift and for negative displacements the elongation growth slowed down when getting close to 1.0% drift. During the first series of cycles to -1.0% drift the elongation at peak displacement for the RW walls ranged between 0.25% and 0.30% of the length of the wall. At +1.0% drift it was around 0.40% and at +2.0% drift it ranged around 0.65% to 0.75% of the wall length.

The peak cyclic elongations for all of the C walls (Figure 13) increased in a linear trend with increasing lateral drift. Comparison amongst walls C1, C2 and C3 that had similar axial loads but different shear-to-span ratios shows that wall C3 had slightly smaller elongations after ±1.5% drift. This wall had a higher shear-to-span ratio, which would have reduced the influence of the shear truss action effect. For walls C1, C4 and C5 that had different axial loads and equal shear-to-span ratios, it can be seen that the increasing axial load had a moderate influence on reducing the axial elongations at peak displacements as the neutral axis depth increased. The confinement reinforcement in wall C6 did not affect elongation at peak displacement, as can be seen when compared to C2 that had similar axial load and the same shear-to-span ratio.

The residual elongations when the walls were unloaded back to zero displacement for all 13 test walls are plotted in Figure 14 to Figure 16 against the maximum lateral drift at the previous peak displacement. The residual elongation developed by the PW walls (Figure 14) was close to zero prior to the failure cycles. This was previously illustrated in Figure 8 where the linear elongation history was shown, and highlights the effect of the axial load applied to the walls. It is worth noting that the walls PW1 and PW3 ($\xi \approx 10\%$) developed higher axial elongation than walls PW2 and PW4 ($\xi \approx 12\%$) when they were beyond ±0.8% drift during the onset of failure. In general, an axial load ratio (ξ) of around 10% appears to be sufficient to effectively close the cracks so that the elongation at peak drifts is fully recovered when the walls were laterally displaced back to a vertical position.

In contrast to the elongation at peak displacements, the residual elongations for the RW walls (Figure 15) progressed symmetrically despite the asymmetry in vertical reinforcement and peak elongations (Figure 12). The residual elongation correlated to the elongation that was produced when the stronger wall end was in tension due to the larger neutral axis and heavier wall end reinforcement that enforced crack closure. Initially, the residual elongations increased quickly and then slowed down between 0.5-1.0% drift. Beyond 1% drift, the residual elongation developed for the wall RWC was larger than the other two, with the wall RWS (lapped splice) producing the lowest residual elongations.

The residual elongations for the C walls (Figure 16) were greater than the other two test series and had a wide scatter between the different walls. The residual elongations in most of the C walls followed a parabolic trend with drift, but wall C1 increased linearly with drift. Walls C1, C2 and C3 showed that residual elongations reduced as the shear-span was increased as the influence of the shear truss action diminished. In addition, walls C1, C4 and C5 showed a significant reduction in the residual elongation as the axial load increased. The residual elongations for wall C1 with an axial load ratio $\xi = 3.5\%$ were 3 times smaller than C4 that had no axial load, and further reduced to almost zero residual elongation when the axial increased to 7.5% for wall C5. As with the peak elongations, the use of transverse reinforcement in the ends of the wall did not show any appreciable difference in the residual elongations when comparing walls C2 and C6.

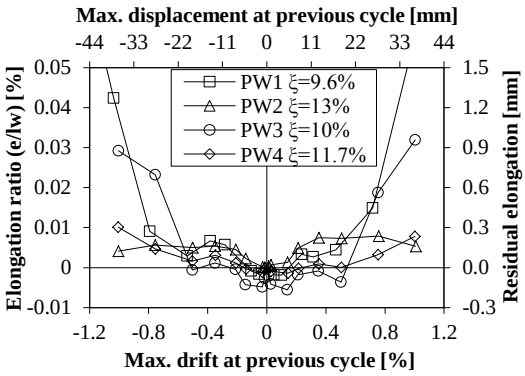

Figure 14: Residual elongations for PW walls.

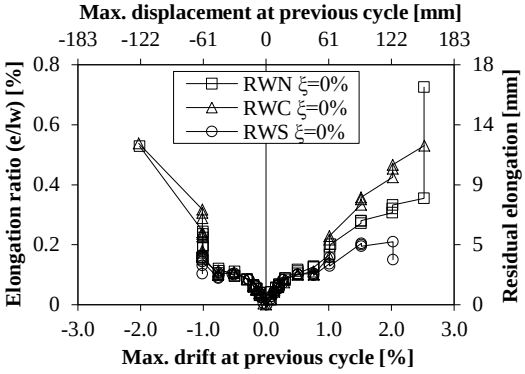

Figure 15: Residual elongations for RW walls.

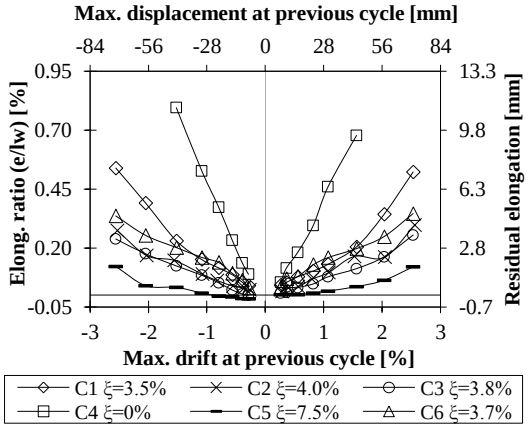

Figure 16: Residual elongations for C walls.

DEVELOPMENT OF NUMERICAL MODELS

Numerical models were developed to simulate the overall wall and axial elongation response of five representative walls from the three test series described above. Two commonly used modelling techniques were investigated, including distributed plasticity fibre-based elements in OpenSees [35] and a membrane finite element approach in VecTor2 [36]. Both of these modelling techniques simulate axial elongation and are employed in various structural analysis software packages. It should be noted that other modelling techniques that use a centreline elements with a lumped plasticity approach (e.g. rotational springs) do not directly account for the axial strains and so are not capable of capturing axial elongation of plastic hinge regions.

Fibre Element Model

The fibre element models represent the walls through uni-linear elements that assume linear strain profiles at each section of the element (plane sections remain plane). As shown in Figure 17, the models consisted of a zero-length element at the base to represent the strain penetration, non-linear elements for the tested portion of the walls, and a linear elastic element for the untested portion of the wall in the cases where the specimen was subjected to moments at the top. The model was constructed using distributed-plasticity fibre-based beam-column elements with force formulation. For all of the tests, the base of the walls was securely fixed to the strong floor and so the bottom node in the numerical models was restrained against lateral displacement and rotation.

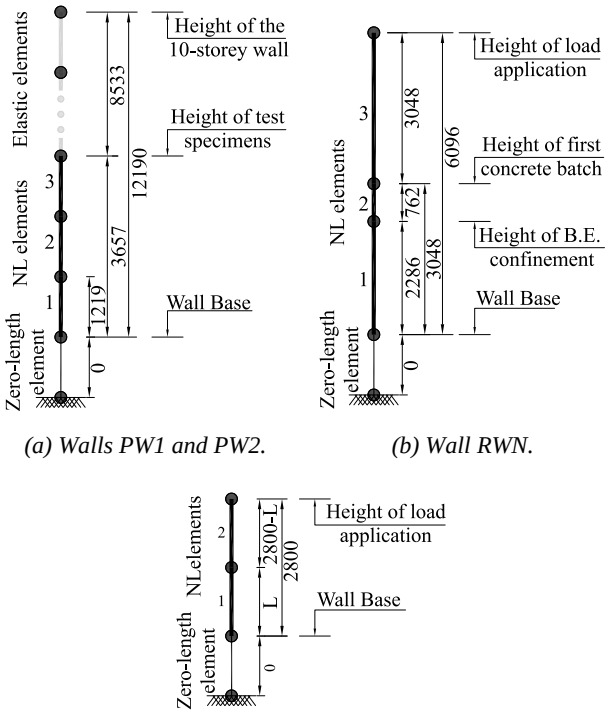

(a) Walls PW1 and PW2. *(b) Wall RWN.*

(c) Walls C1 and C5.

Figure 17: Schematic representation of fibre-element models in OpenSees (mm).

Figure 17(a) presents a schematic representation of PW1 and PW2. The model meshing consisted of 3 elements to represent the tested portion of the wall, allowing for load application points and different section definitions. The element length was 1219 mm and used 3 integration points to capture the spread of plasticity within the element. Gauss-Lobbato scheme was selected as the integration scheme of the elements. Fibre discretisation of the cross section corresponded to 40 fibres along the confined wall ends and 150 fibres along the web region.

Figure 17(b) represents the numerical model for the RWN wall. Again, 3 elements were used to represent the wall with the lengths shown in the figure. The elements lengths allowed for different material properties (wall cast in two lifts), different section definition (allow for height of confinement) and loading points. Integration points to capture the spread of plasticity were defined as 6, 2 and 5 for elements 1, 2 and 3 respectively and a Gauss-Lobbato integration scheme was used. The left confined wall end was divided into 30 fibres,

the right confined wall end was divided into 20 fibres and the web region was divided into 290 fibres.

Figure 17(c) present the numerical model for walls C1 and C5. Due to softening behaviour of these walls, element meshing was selected as to overcome localisation issues [37]. The element length (L) was selected following the regularisation technique proposed by Scott and Fenves [38] along with the crushing energy proposed by Pugh, Lowes and Lehman [39]. This technique states that the weight of the integration points should be selected to match the length of the equivalent plastic hinge. Consequently, and considering the height of the walls and their reinforcement layout, the length of the first element of each wall was determined by the weight of a Gauss-Lobbato integration scheme for an element with two integration points. The second element on each model had 3 integration points and the complementary length to reach the test specimens' height. Concrete matrix was discretised with 45 fibres for the confined wall end and 170 fibres for web region.

In addition to the fibre-section definition that accounts for the axial-flexural deformation, shear and strain penetration were also included in the model. Since the walls investigated were flexure-dominant, shear deformations were approximately included by the aggregation of an elastic material with elastic modulus equal to $0.41E_c$ to the fibre section. It is important to mention that this approach does not consider shear-flexure interaction, instead it adds a lateral deformation component according to the elastic shear stiffness, and as a consequence the truss action effect is not included when determining elongation. Strain penetration and bond slip were included in the model using the recommendations proposed by Zhao and Sritharan [40]. These recommendations consisted of a zero-length fibre-based element at the base of the wall with modified concrete and steel materials. The modified concrete material is defined with modified post peak strength envelope to allow for high strain levels with low reduction in strength. The steel fibres are represented by a strain penetration material model, which consisted of a relationship between the stress and the total slip of the bar at the wall-foundation interface.

Uniaxial constitutive material models were utilised to describe the nonlinear material behaviour of the fibres, and P-Delta geometric transformation was used to represent the nonlinear geometric behaviour. Graphical representations of both the concrete and steel material models are shown in Figure 18. The concrete stress-strain response was defined based on the Chang and Mander concrete model modified by Waugh [41] and available in OpenSees as Concrete07. This concrete model was selected as it allows for wedging action in the cracks and provides a robust hysteretic behaviour that considers both complete or partial unloading and reloading cycles. The concrete model uses Tsai's equation [42] to describe the envelope curves for compression and tension and uses a simplified trilinear curve for unloading and reloading.

The reinforcing steel was simulated using the Menegotto and Pinto [43] model, modified by Filippou, Popov and Vertero [44] to include isotropic strain hardening and available in OpenSees as Steel02. The stress-strain relationship of Steel02 is described by a linear elastic curve with slope E_0 (steel's elastic modulus) and then, when close to yielding, curves and follows an asymptote with slope $b \cdot E_0$ (strain hardening slope; $b<1$). The unloading and reloading path accounts for Bauschinger effects.

Input parameters for the unconfined concrete properties and reinforcing steel properties were based on material test results for each wall. The confined concrete properties were calculated according to the model proposed by Mander et al. [45]. When measured material properties were not available, nominal values were assumed and material constitutive models were obtained from Collins and Mitchell [46] for unconfined concrete in compression and from the fib 2010 Model code [47] for concrete tensile strength. Material definitions were assigned to the corresponding fibres according to their actual position in the wall cross-section.

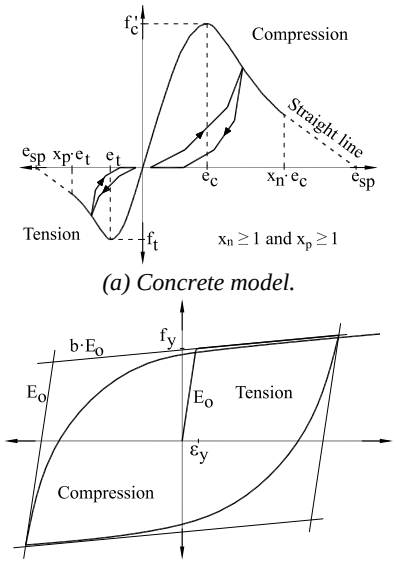

Figure 18: Schematic representation of the material models used in OpenSees.

The RC walls were tested with reverse cyclic loading and so the simulation was conducted using a sequence of pushover analyses that replicated the displacement history of the top of the experimental walls. The first analysis step applied the gravity loads to the models and then the cyclic pushover was conducted by pushing the walls to a series of lateral displacement, as per the loading protocol applied during the tests.

Membrane Element Model (FEM)

The membrane element model was developed in VecTor2. In contrast to fibre-based element models that assume a linear strain profile, the membrane elements in VecTor2 consider axial-shear-flexure interaction. Schematic representations of the VecTor2 models are illustrated in Figure 19. All the models were built using four-node plane stress rectangular elements for the concrete. Horizontal and transverse reinforcement were modelled as smeared reinforcement, whereas two-node truss element with uniform cross-sectional area was used to model the vertical reinforcement. No bond slip was considered between reinforcement and the surrounding concrete. A foundation that was fixed for translation and rotation at base was modelled to simulate the concrete foundation in the test. The vertical reinforcement extended from the wall to the bottom of the foundation to simulate the anchorage of the vertical reinforcement. The mesh size was adjusted for each test series based on a sensitivity study [48]. For the C walls, a mesh size of 75×75 mm was chosen to best represent the global and local behaviour of the test walls with no premature localisation failures. For the PW and RWN walls, the mesh size of approximately 100×100 mm was considered appropriate to capture the wall behaviour.

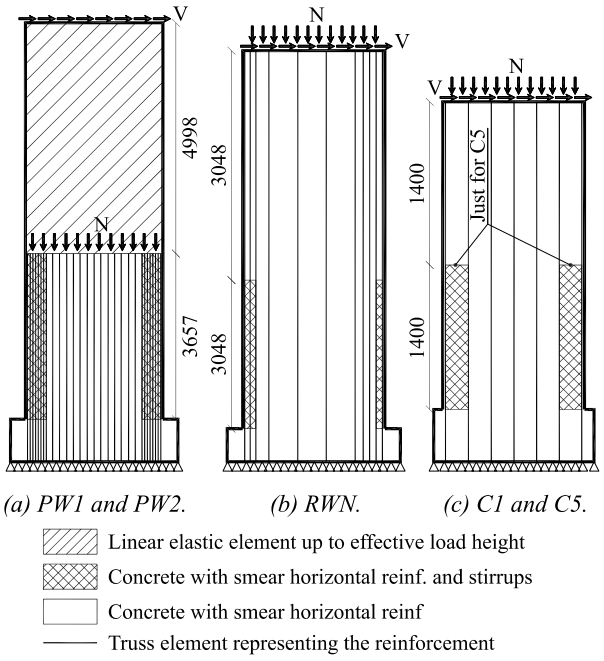

(a) PW1 and PW2. *(b) RWN.* *(c) C1 and C5.*

Figure 19: Schematic representation of membrane element models in VecTor2 (mm).

The applied load conditions were different for each wall model. For the PW walls, the test walls were subjected to a combination of horizontal force, axial load and bending moment at the top of the test wall to represent a multi-story building wall. The model represented the full height of the wall, as shown in Figure 19(a), with the upper part of the wall modelled as an elastic element with a modulus of elasticity 1000 times bigger than the concrete elastic modulus. The height of the elastic region was calculated according to the shear-to-span ratio that was applied during the test. The lateral load was applied at the top of the model but the drift of the wall was controlled at the same height of the test walls. For wall RWN, the loading height was slightly lower than the full height of the test walls, and so this horizontal loading point was kept consistent between the model and the test. A rigid beam was fixed at the top of the C wall models to simulate the loading beam attached during testing. Horizontal load was applied to the rigid beam element and the loading height was the same as the test to represent the applied shear-to-span ratio. For all the walls, the modelled lateral drifts and shear span were identical to the loading protocols that were applied during the test. When needed, an axial load was applied uniformly on the top of the wall and kept constant throughout the entire analysis.

The steel constitutive material was simulated using the Seckin model [36]. As show in Figure 20(b), this model included the elastic portion until yield, a yield plateau, and a polynomial curve representing the strain hardening behaviour, and accounted for Bauschinger effects in addition to buckling using the Dhakal and Maekawa model [49]. The concrete material representation is shown in Figure 20(a) and used a Kent-Park stress-strain relationship for the compression envelope which consisted of a parabolic ascending branch until peak stress followed by a linear descending branch. The concrete hysteresis behaviour was implemented using Palermo and Vecchio [50]. Both the ascending and descending branches considered the effects provided by the confining reinforcement. In tension, as can be seen in Figure 20(a), the Lee et al. [36] model was used to represent the stress-strain envelope. The input of compression strength for all the wall models was based on the measured mechanical properties of compression cylinder tests. As with the fibre-models, the fib 2010 Model code [47] recommendations for concrete tensile strength were used for the PW and RWN walls. For the C test walls, the tensile strengths were based on those measured from split cylinder tensile tests.

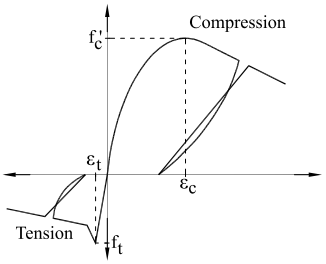

(a) Concrete model.

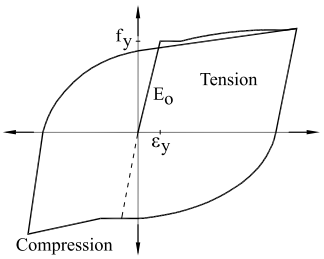

(b) Steel model.

Figure 20: Schematic representation of material models used in VecTor2.

SIMULATION OF WALL ELONGATION

The proposed fibre and membrane (FEM) element models were compared against the experimental results from five of the test walls (PW1, PW2, RWN, C1, C5). Only the comparison of the global moment-drift response and the axial elongations are shown due to space limitations and additional validation of similar models against a wider range of global and local response parameters has been published elsewhere [33, 39]. The models were not intended to capture failure modes of each specimen, and so were only investigated over the reliable range of the test data prior to any degradation due to crushing, reinforcement buckling or reinforcement fracture.

Lateral Load Response

The global base moment vs. lateral drift response for each of the five modelled walls are compared with the test results in Figure 21. Overall both numerical models were able to capture the wall response with good accuracy, closely matching the envelope nonlinear strength development as well as the initial stiffness of the walls. The transition curves from a positive peak displacement to a negative peak displacement were better simulated by the fibre element models, highlighting the relevance of considering a concrete material model with the ability to appropriately simulate crack closure. This is particularly noticeable for walls C1 and C5, where the membrane FEM model shows increased pinching in the response when compared to the test and fibre models. These lightly reinforced concrete walls were dominated by wide crack openings and the ability of the fibre model to simulate the compression stress transfer across cracks that are not fully closed resulted in a better representation of the wall hysteresis response.

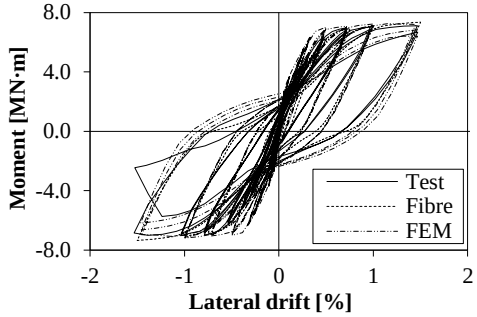

(a) Wall PW1.

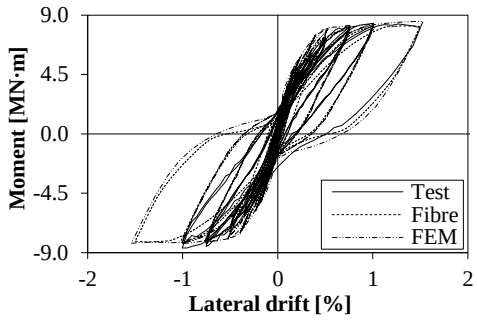

(b) Wall PW2.

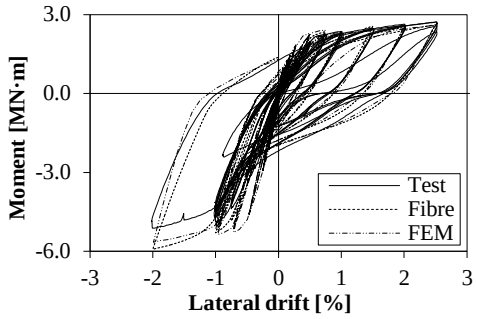

(c) Wall RWN.

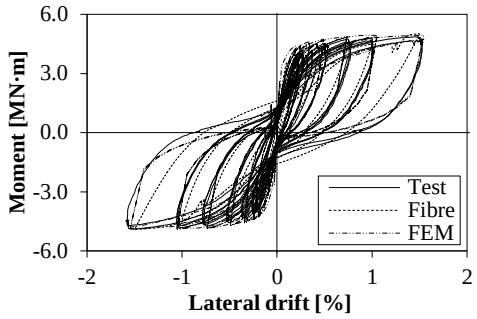

(d) Wall C1.

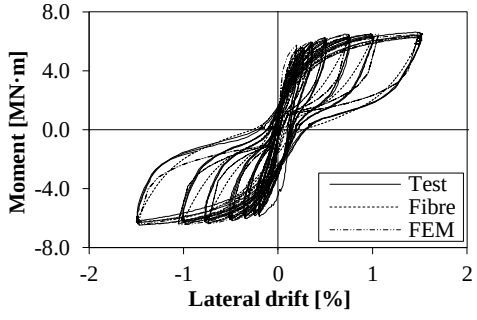

(e) Wall C5.

Figure 21: Moment-Displacement response for both models.

Cyclic Elongation History

The cyclic elongation history for both models is compared against the results of the five test walls in Figure 22. The numerical models were both able to simulate the overall behaviour and cyclic development of the wall elongation. The calculated elongations increased with drift and decreased when returning to zero lateral displacement, which allowed the model to simulate both the elongation at peak displacements and the residual elongation at zero displacement. In the case of the numerical models for PW1 and PW2, the experimental cyclic elongation history was consistently matched by the fibre element models, while it was generally over predicted by the membrane FEM models. The fibre element models for the RWN wall represented the asymmetric cyclic elongation development, but under predicted the elongation during small lateral drift cycles. The membrane FEM model for the RWN wall produced a somewhat symmetric cyclic development and over predicted the wall elongations during larger drift cycles. In the case of walls C1 and C5, both models under predicted the cyclic elongation development for wall C1, whereas their prediction for wall C5 matched the experimental response with good accuracy. For wall C1, the experimental elongation response showed significant accumulations during cycles. This accumulation was partially captured by the fibre element model, but the membrane FEM element simulation showed no significant accumulation of residual elongations.

Peak Elongations

To investigate the elongation response in more detail, the envelope of the simulation of elongation at peak cyclic displacements is compared against the experimental results in Figure 23. The fibre element models simulated the peak elongations for walls PW1 and PW2 with good accuracy, whereas the membrane FEM models over predicted the peak elongations by more than 30% at 1% lateral drift. In the case of the RWN wall, the peak elongations were slightly under predicted by the fibre model and slightly over predicted by the membrane FEM model. The asymmetric shape of the RWN elongation envelope was not captured by the membrane model, which produced fairly symmetrical envelopes for both positive and negative lateral drifts. For walls C1 and C5, both models estimated similar peak elongations. For wall C1 the peak elongations were consistently underestimated by approximately 20% for both numerical models. The peak elongations for wall C5 were accurately predicted by both models.

Residual Elongations

Comparisons of the calculated residual elongations after unloading back to zero lateral displacement are shown in Figure 24 (note that residual elongation is plotted against the maximum lateral drift at previous peak displacement). For the PW and RW walls, both models captured the residual elongations with reasonable accuracy. It should be noted that the residual elongation for PW2 was extremely small (less than 0.3 mm) and as a result of these small values residual elongations were difficult to predict precisely. For the C walls, the fibre element models captured the experimental residual elongation with acceptable accuracy, whereas the membrane FEM models calculated zero residual elongation for both walls modelled.

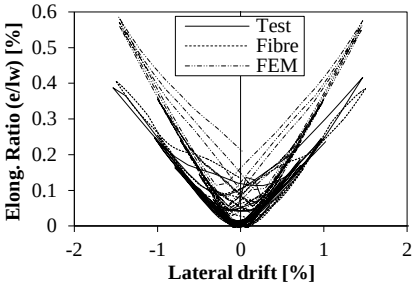

(a) Wall PW1.

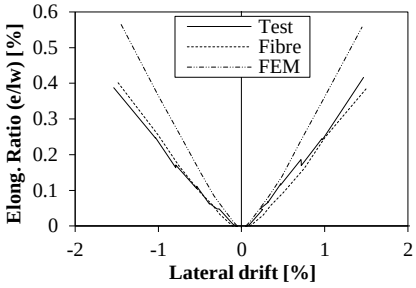

(a) Wall PW1.

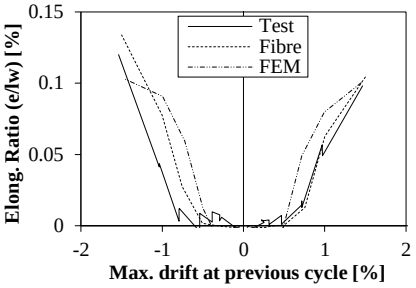

(a) Wall PW1.

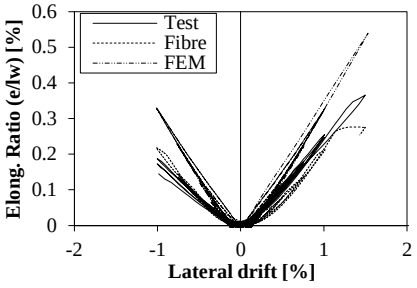

(b) Wall PW2.

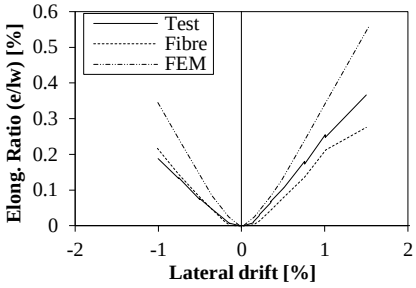

(b) Wall PW2.

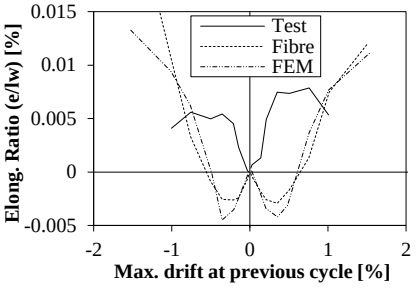

(b) Wall PW2.

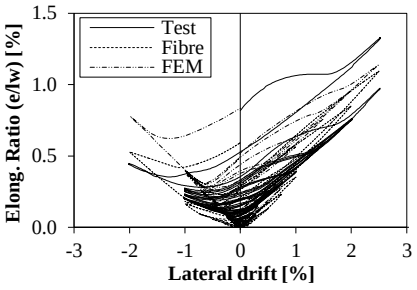

(c) Wall RWN.

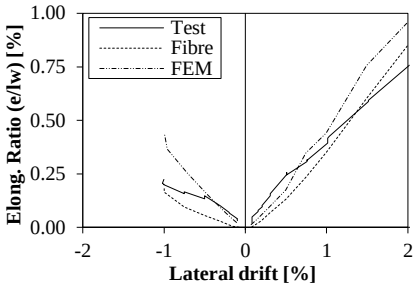

(c) Wall RWN.

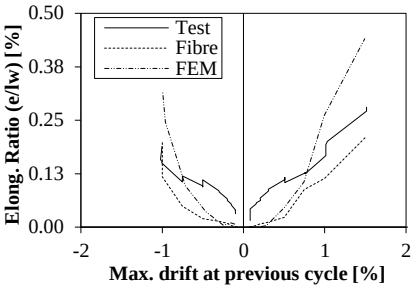

(c) Wall RWN.

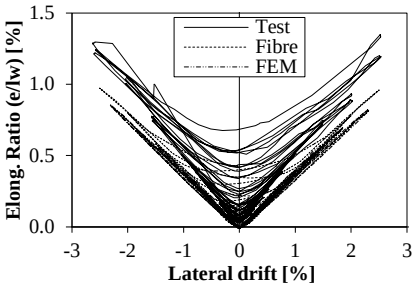

(d) Wall C1.

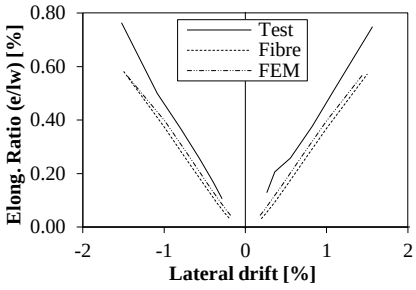

(d) Wall C1.

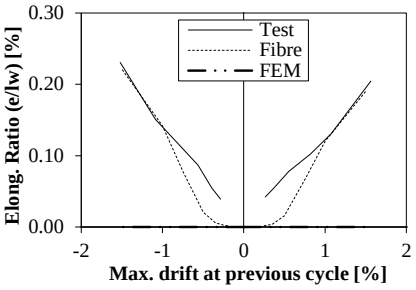

(d) Wall C1.

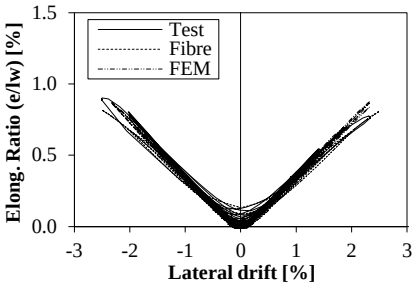

(e) Wall C5.

Figure 22: Comparison of cyclic elongation for both models.

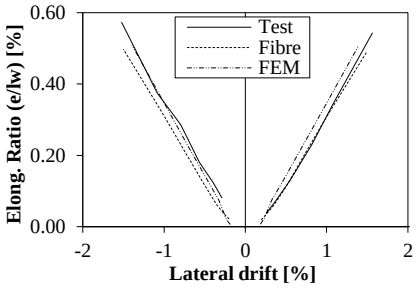

(e) Wall C5.

Figure 23: Comparison of peak elongations for both models.

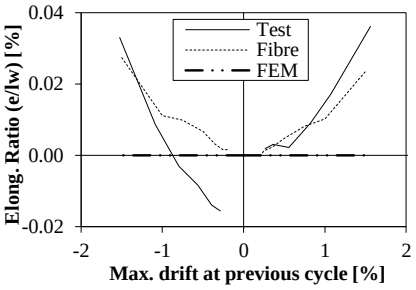

(e) Wall C5.

Figure 24: Comparison of residual elongations for both models.

Modelling Elongation in RC Walls

The peak elongations are predominantly a function of the geometric elongation, and to a lesser extend the residual crack widths and plastic strains in the compression end of the wall. Given that the walls modelled were all flexure dominant, it is not surprising that both the fibre element and membrane element models could capture the peak elongations with reasonable accuracy. Both models provided appropriate representation of the wall axial strains, curvatures, and neutral axis depth which led to good estimation of the geometric elongation. The residual elongations are a function of the permanent accumulated elongation that is related to reinforcement compression strains, crack closure, and truss action. The formulation of fibre-based elements does not include flexure-shear interaction and so cannot capture the effects of truss action. However, the advanced concrete material models available in OpenSees are capable of accurately representing stresses in partially closured cracks. The membrane element model accounts for the truss action as plane sections are not required to remain plane, but the more simplified concrete hysteresis models in VecTor2 do not account for crack closure stresses.

The differences in the model formulation and material models were clearly evident from the residual elongation results. The ability of the fibre element model to capture the residual elongations in all walls highlighted that for flexure dominant walls, truss action was not significant to the elongation response. Both models could also capture the residual elongations in the PW and RW walls. This finding indicates that the larger vertical reinforcement contents in the PW or RW walls meant that the plastic strains in the compression reinforcement were more significant to the residual crack widths than the crack closure stresses, even when moderate axial loads were applied. However, the inability of the VecTor2 membrane element model to capture residual elongations for walls C1 and C5 highlighted that the crack closure model was critical for these walls. The light vertical reinforcement and moderate axial loads for the C walls meant that the stresses that develop in partially closed cracks were significant to the wall elongation response.

To investigate the significance of the crack closure model on the response of wall C5, different concrete material models were trialled using the fibre element model. The alternative concrete material selected was Concrete02, a modified Kent-Park material model defined as per Yassin [51], which was similar to that implemented in VecTor2. The calculated residual elongations for the wall C5 with the fibre element model using both Concrete02 and Concrete07 are shown in Figure 25. It can be seen that similarly to the results of the membrane element model, the fibre element model also predicted zero residual elongation when using the Concrete02 model that did not include partial crack closure stresses.

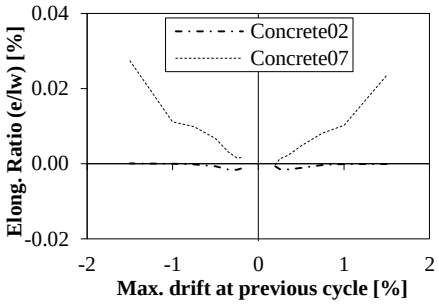

Figure 25: Residual elongation for wall C5 using Concrete02 and Concrete07.

CONCLUSIONS

As with other RC members, plastic hinges in RC walls develop axial elongations. The elongation response is dependent on the wall section (vertical reinforcement layout, reinforcement ratios) and the applied loading (cyclic load history and axial loads). A total of 13 previously tested rectangular RC walls with flexure-dominant behaviour were investigated to understand the magnitude of elongations that developed and the influence of key parameters. In addition, two commonly used numerical modelling techniques were used to simulate the test wall behaviour and verify the ability of the models to capture axial elongations. Based on the analysis performed the following conclusions were drawn:

- The axial elongations in the analysed rectangular flexure-dominant RC walls ranged between 0.4% and 0.8% of the wall length when subjected to 1.5% lateral drift.
- Similar to what has been observed previously for RC frames, axial compression reduced the total elongation that developed in the test walls. It was observed that an axial load ratio of about ξ = 10% reduced the residual elongation to almost zero.
- An asymmetric vertical reinforcement layout produced asymmetric peak elongations, with higher elongations when the weaker end of the wall was in tension. However, the residual elongations developed symmetrically and were controlled by the elongation produced when the strongest wall end was in tension.
- Elongations produced in lightly reinforced concrete walls were larger than the elongations produced in the more heavily reinforced RC walls due to greater influence of residual crack widths and the small neutral axis depth.
- The provisions for estimating wall axial elongation that have been proposed for inclusion in the New Zealand Concrete Structures Standard (NZS 3101:2006 A3-draft) were found to provide acceptable predictions of the magnitude of axial elongation in RC walls.
- The numerical models as described here were able to capture the global wall response and the peak axial elongations of the selected rectangular ductile walls with reasonable accuracy. The first model, based on fibre sections, simulated elongations within 5-10% accuracy for all the walls with the exception of wall C1 which was within 20% of accuracy. The second model, based on membrane elements, simulated elongation within 5-10% accuracy for wall C5, within 20% for wall C1, and within 30-40% for the remaining walls.
- The utilisation of a concrete material model that was able to account for stresses transferred across partially closed cracks was essential to accurately predict the residual elongation in the lightly reinforced concrete walls.

ACKNOWLEDGMENTS

The authors wish to acknowledge the Chilean Government (BecasChile scholarship) and the China Scholarship Council for supporting the doctoral studies of the first two authors, respectively. Financial support for this research was also provided by the Natural Hazards Research Platform. Part of the experimental data used during this investigation was downloaded from the NEES Hub data repository, listed as project number NEES-2005-0022 and NEES-2005-0104.

REFERENCES

1. Fenwick RC and Megget LM (1993). "Elongation and Load Deflection Characteristics of Reinforced Concrete Members Containing Plastic Hinges". *Bulletin of the NZSEE*, **26**(1): 28-41.

2. Wuu PJ (1996). "*Deformations in Plastic Hinge Zone of R/C Beam in Ductile Frame Structures Subjected to Inelastic Cyclic Loading*". Master Thesis, University of Auckland, Auckland, New Zealand, 83 pp.
3. Cheung PC (1991). "*Seismic Design of Reinforced Concrete Beam-Colum Joints with Floor Slab*". PhD Dissertation, Univeristy of Canterbury, Christchurch, New Zealand, 397 pp.
4. Douglas KT (1992). "*Elongation in Reinforced Concrete Frames*". Report No. 526, University of Auckland, Auckland, New Zealand, 92 pp.
5. Restrepo-Posada JI (1992). "*Seismic Behaviour of Connections Between Precast Concrete Elements*". PhD Dissertation, University of Canterbury, Christchurch, New Zealand, 412 pp.
6. McBride AP (1995). "*Elongation of Reinforced Concrete Beam-Column Units with and without Slab*". Master Thesis, University of Auckland, Auckland, New Zealand, 115 pp.
7. Lau DBN, Fenwick RC and Davidson BJ (2002). "Seismic Performance of RC Perimeter Frames with Slabs Containing Prestressed Units". *NZSEE Annual Conference*, Napier, New Zealand, 15-17 March.
8. Fenwick RC, Bull D, MacPherson C and Lindsay R (2006). "The Influence of Diaphragms on Strength of Beams". *NZSEE Annual Conference*, Napier, New Zealand, 10-12 March.
9. MacPherson C, Mander JB and Bull D (2005). "Reinforced Concrete Seating Details of Hollow-Core Floor Systems". *NZSEE Annual Conference*, Taupo, New Zealand, 11-13 March.
10. Fenwick RC and Davidson BJ (1995). "Elongation in Ductile Seismic-Resistant Reinforced Concrete Frames". *Thomas Paulay Symposium*, **SP-157**: 143-170.
11. Peng BHH, Dhakal RP, Fenwick RC, Carr AJ and Bull D (2013). "Multispring Hinge Element for Reinforced Concrete Frame Analysis". *Journal of Structural Engineering*, **139**(4): 595-606.
12. Malcolm R (2015). "*Seismic Performance of Reinforced Cocrete Coupled Walls*". Master Thesis, University of Auckland, Auckland, New Zealand, 180 pp.
13. Wight JK (1985), "*Earthquake Effects on Reinforced Concrete Structures: U.S.-Japan Research*", SP-84, American Concrete Institute, Detroit, U.S.A.
14. Chesi C and Schnobrich WC (1987). "*3-Dimensional Contribution to Frame-Wall Lateral Behavior*". Report No. 531, University of Illinois, Urbana-Champaign, U.S.A., 50 pp.
15. Canterbury Earthquake Royal Commission (2012). "*Final Report, Volume 2: The Performance of the Christchurch CBD Buildings*". Wellington, New Zealand, 239 pp.
16. SESOC (2013). "*Interim Design Guidelines: Design of Conventional Structural Systems Following the Canterbury Earthquakes*". SESOC, Wellington, New Zealand, 49 pp.
17. Standards New Zealand (2014). "*Public Comment Draft NZS 3101:2006 Concrete Structures Standard Part 1 (Standard) Amendment No. 3*". Standards New Zealand, Wellington, New Zealand, 67 pp.
18. Fenwick RC and Fong A (1979). "The Behaviour of Reinforced Concrete Beams under Cyclic Loading". *Bulletin of the New Zealand National Society for Earthquake Engineering*, **12**(3): 158-167.
19. Fenwick RC and Thom CW (1982). "*Shear Deformation in RC Beams Subjected to Inelastic Cyclic Loading*". Report No. 279, University of Auckland, Auckland, New Zealand, 58 pp.
20. Megget LM and Fenwick RC (1989). "Seismic Behavior of a Reinforced Concrete Portal Frame Sustaining Gravity Loads". *Bulletin of the New Zealand Society for Earthquake Engineering*, **22**(1): 39-49.
21. Zerbe HE and Durrani AJ (1989). "Seismic Response of Connections in Two-Bay R/C Frame Subassemblies". *Journal of Structural Engineering*, **115**(11): 2829-2844.
22. Cooper M, Davidson BJ and Ingham J (2005). "The Influence of axial Compression on the Elongation of Plastic Hinges in Reinforced Concrete Beams". *The New Zealand Concrete Industries Conference 2005*, Auckland, New Zealand, 22-24 September.
23. Matthews JG, Mander JB and Bull DK (2004). "Prediction of Beam Elongation in Structural Concrete Members using a Rainflow Method". *NZSEE Annual Conference*, Rotorua, New Zealand.
24. Lee J and Watanabe F (2003). "Shear Deterioration of Reinforced Concrete Beams Subjected to Reversed Cyclic Loading". *ACI Structural Journal*, **100**(4): 480-489.
25. Davidson BJ and Fenwick RC (1993). "*The Seismic Response of Ductile Reinforced Concrete Frames with Uni-directional Hinges*". Report No. 527, University of Auckland, Auckland, New Zealand, 59 pp.
26. Kabeyasawa T, Sanada Y and Maeda M (2000). "Effect of Beam Axial Deformation on Column Shear in Reinforced Concrete Frames". *12th World Conference on Earthquake Engineering*, Auckland, New Zealand, 30 January - 4 February.
27. Kim J, Stanton J and MacRae G (2004). "Effect of Beam Growth on Reinforced Concrete Frames". *Journal of Structural Engineering*, **130**(9): 1333-1342.
28. Eom T, Park H, Kim J and Lee H (2013). "Web Crushing and Deformation Capacity of Low-Rise Walls Subjected to Cyclic Loading". *Structural Journal*, **110**(4): 575-584.
29. Birely A (2012). "*Seismic Performance of Slender Reinforced Concrete Structural Walls*". PhD Dissertation, University of Washington, Washington, U.S.A., 983 pp.
30. Lowes L, Lehman D, Birely A, Kuchma DA, Hart CR and Marley K (2011). "*Behavior, Analysis, and Design of Complex Wall Systems: Planar Wall Test Program Summary Document*". University of Washington and University of Illinois (Urbana-Champaign), 87 pp.
31. Aaleti S, Brueggen BL, Johnson B, French C and Sritharan S (2013). "Cyclic Response of Reinforced Concrete Walls with Different Anchorage Details: Experimental Investigation". *Journal of Structural Engineering*, **139**: 1181-1191.
32. Johnson BM (2007). "*Longitudinal Reinforcement Anchorage Detailing Effects on RC Structural Wall Behavior*". Master Thesis, University of Minnesota, Minneapolis, U.S.A., 354 pp.
33. Lu Y, Henry RS, Gultom R and Ma TQ (In-press). "Cyclic Testing of Reinforced Concrete Walls with Distributed Minimum Vertical Reinforcement". *Journal of Structural Engineering*.
34. Bentz EC and Collins MP (2001). *"Response-2000 (Software)"*. University of Toronto, Toronto, Canada.
35. Mazzoni S, McKenna F, Scott MH and Fenves GL (2006). *"Open System for Earthquake Engineering Simulation (OpenSees Software)"*. Pacific Earthquake Engineering Research Center, University of California, Berkeley, U.S.A.

36. Wong YC and Vecchio FJ (2006). *"VecTor2 (Software)"*. University of Toronto, Toronto, Canada.
37. Coleman J and Spacone E (2001). "Localization Issues in Force-Based Frames Elements". *Journal of Structural Engineering*, **127**(11): 1257-1265.
38. Scott MH and Fenves GL (2006). "Plastic Hinge Integration Methods for Force-Based Beam-Column Elements". *Journal of Structural Engineering*, **132**(2): 244-252.
39. Pugh JS, Lowes L and Lehman D (2015). "Nonlinear Line-Element Modeling of Flexural Reinforced Concrete Walls". *Engineering Structures*, **104**: 174-192.
40. Zhao J and Sritharan S (2007). "Modeling of Strain Penetration Effects in Fiber-Based Analysis of Reinforced Concrete Structures". *ACI Structural Journal*, **104**(2): 133-141.
41. Waugh J, Aaleti S, Sritharan S and Zhao J (2008). "*Nonlinear Analysis of Rectangular and T-Shaped Concrete Walls*". ERI-09327, Iowa State University, Iowa, U.S.A., 351 pp.
42. Tsai W (1988). "Uniaxial Compressional Stress-Strain Relation of Concrete". *Journal of Structural Engineering*, **114**(9): 2133-2136.
43. Menegotto M and Pinto PE (1973). "Method of Analysis for Cyclically Loaded R.C. Plane Frames Including Changes in Geometry and Non-Elastic Behaviour of Elements under Combined Normal Force and Bending". *IABSE Symposium of Resistance and Ultimate Deformability of Structures Acted on by Well-defined Repeated Loads*, Lisbon, Portugal.
44. Filippou FC, Popov EP and Bertero VV (1983). "*Effects of Bond Deterioration on Hyteretic Behavior of Reinforced Concrete Joints*". Report UCB/EERC-83/19, University of California, Berkeley, U.S.A., 212 pp.
45. Mander JB, Priestley MJN and Park R (1988). "Theoretical Stress-Strain Model for Confined Concrete". *Journal of Structural Engineering*, **114**(8): 1804-1826.
46. Collins MP and Mitchell D (1997), "*Prestressed Concrete Structures*". Response Publications, Toronto, Ontario, 766 pp.
47. Fédération Internationale du Béton (2010). "*Model Code 2010 - Volume 1*". Fédération Internationale du Béton, Lausanne, Switzerland, 357 pp.
48. Lu Y (2016). "*Seismic Design of Lightly Reinforced Concrete Walls*". PhD Dissertation, University of Auckland, Auckland, New Zealand, 319 pp.
49. Dhakal RP and Maekawa K (2002b). "Path-dependent Cyclic Stress-strain Relationship of Reinforcing Bar Including Buckling". *Engineering Structures*, **24**(11): 1383-1396.
50. Palermo D and Vecchio FJ (2007). "Simulation of Cyclically Loaded Concrete Structures Based on the Finite-Element Method". *Journal of Structural Engineering*, **133**(5): 728-738.
51. Yassin MH (1994). "*Nonlinear Analysis of Prestressed Concrete Structures under Monotonic and Cyclic Loads*". PhD Dissertation, University of California, Berkeley, U.S.A., 206 pp.